nature nanotechnology

LETTERS

PUBLISHED ONLINE: 23 MARCH 2015 | DOI: 10.1038/NNANO.2015.36

Graphene-templated directional growth of an inorganic nanowire

Won Chul Lee[1,2†], Kwanpyo Kim[3,4†], Jungwon Park[5,6†], Jahyun Koo[7], Hu Young Jeong[8], Hoonkyung Lee[7], David A. Weitz[5,6], Alex Zettl[3,9*] and Shoji Takeuchi[1,2*]

Assembling inorganic nanomaterials on graphene[1–3] is of interest in the development of nanodevices and nanocomposite materials, and the ability to align such inorganic nanomaterials on the graphene surface is expected to lead to improved functionalities[4], as has previously been demonstrated with organic nanomaterials epitaxially aligned on graphitic surfaces[5–10]. However, because graphene is chemically inert, it is difficult to precisely assemble inorganic nanomaterials on pristine graphene[2,11–16]. Previous techniques[2,3] based on dangling bonds of damaged graphene[11,17–20], intermediate seed materials[11,15,16,21,22] and vapour-phase deposition at high temperature[12–14,23–25] have only formed randomly oriented or poorly aligned inorganic nanostructures. Here, we show that inorganic nanowires of gold(I) cyanide can grow directly on pristine graphene, aligning themselves with the zigzag lattice directions of the graphene. The nanowires are synthesized through a self-organized growth process in aqueous solution at room temperature, which indicates that the inorganic material spontaneously binds to the pristine graphene surface. First-principles calculations suggest that this assembly originates from lattice matching and π interaction to gold atoms. Using the synthesized nanowires as templates, we also fabricate nanostructures with controlled crystal orientations such as graphene nanoribbons with zigzag-edged directions.

The nanowires were synthesized by incubating single-layered graphene and solid gold simultaneously in an aqueous solution of 250 mM ammonium persulphate, $(NH_4)_2S_2O_8$, at room temperature for 17 h (Fig. 1a). Various types of gold precursor, such as gold nanoparticles or gold microstructures, can be used in this reaction depending on the experimental goal. The acidic solution of ammonium persulphate oxidizes gold precursors to form nanowires. Graphene, as both a substrate and template for nanowire growth, is floated on the reaction solution, thus providing a surface on which the nucleation and growth of nanowires can occur (Supplementary Methods and Supplementary Fig. 1).

During this incubation, the nanowires grow on the graphene surfaces along the specific lattice directions of the graphene. Typical transmission electron microscopy (TEM) images of the graphene/nanowire samples (Fig. 1b and Supplementary Fig. 2a,b) show horizontally grown nanowires on the surfaces. Measurements obtained using TEM and atomic force microscopy (AFM) indicate that the nanowires are in the form of nanoribbons lying on the graphene surfaces, with length, width and thickness of 94.7 ± 42.2 nm, 10.1 ± 5.0 nm and 3.29 ± 0.47 nm, respectively (Supplementary Fig. 3). Interestingly, the synthesized nanowires are preferentially oriented along three directions with rotations of 120° relative to one another (Fig. 1b and Supplementary Fig. 2a–d). From the observed symmetry of the nanowire axis directions, we expected the nanowires to have preferential growth directions that are related to the underlying graphene lattice structures. Indeed, a selected area electron diffraction (SAED) pattern (inset in Fig. 1b) of the samples clearly shows this epitaxial relationship between the nanowires and graphene. The nanowire axis directions in Fig. 1b show good orientational alignment to the second-order diffraction peaks—(1–210) peaks—of graphene (circled in red). This alignment, which is also confirmed statistically (Fig. 1d), indicates that the nanowire directions coincide with the zigzag lattice directions of the underlying graphene in real lattice space. In addition, the diffraction peaks from the nanowires (circled in yellow) are aligned to graphene's (1–210) peaks in the SAED pattern. Together with high-resolution TEM images and their Fourier transforms (Fig. 1c and Supplementary Fig. 2e,f), the SAED pattern shows that each nanowire is single crystalline and that the crystal lattices of the nanowires and graphene are rotationally aligned. An atomic-resolution TEM image (Fig. 1e,f) also directly confirms the nanowire alignment on the graphene, with the nanowire axis aligned along the zigzag lattice direction of the graphene lattice.

This nanowire alignment enables us to easily visualize the crystal directions and grain boundaries in polycrystalline graphene using TEM or even scanning electron microscopy (SEM), as shown in Fig. 1g,h. Because the nanowire axes directly represent the crystal directions of the underlying graphene, tilt grain boundaries in the graphene can be identified by changes in the nanowire axis directions (Fig. 1i). Previously, atomic-resolution imaging tools such as TEM and scanning tunnelling microscopy (STM) have been used to directly image the crystal directions and grain boundaries of graphene[26]. However, these imaging processes often involve special sample preparation or substrate requirements and can be time-consuming. The present SEM-based imaging provides a facile tool to monitor crystal directions and graphene grain boundaries (with a spatial resolution of ~100 nm in Supplementary Fig. 4), which is essential for studying the polycrystallinity of graphene and its implications for various properties.

We identified the nanowire material as gold(I) cyanide[27] (AuCN) based on our elemental analysis and atomic structure characterizations. Elemental analyses including energy-dispersive X-ray spectroscopy (EDX) and electron energy loss spectroscopy (EELS) (Supplementary Figs 5 and 6) confirm the presence of Au and N,

[1]Institute of Industrial Science, The University of Tokyo, Tokyo 153-8505, Japan. [2]ERATO Takeuchi Biohybrid Innovation Project, Japan Science and Technology Agency, Tokyo 153-8904, Japan. [3]Department of Physics, University of California at Berkeley, Berkeley, California 94720, USA. [4]Department of Physics, Ulsan National Institute of Science and Technology (UNIST), Ulsan 689-798, South Korea. [5]School of Engineering and Applied Sciences, Harvard University, Cambridge, Massachusetts 02138, USA. [6]Department of Physics, Harvard University, Cambridge, Massachusetts 02138, USA. [7]Department of Physics, Konkuk University, Seoul 143-701, South Korea. [8]UNIST Central Research Facilities (UCRF), Ulsan National Institute of Science and Technology (UNIST), Ulsan 689-798, South Korea. [9]Materials Sciences Division, Lawrence Berkeley National Laboratory, Berkeley, California 94720, USA. †These authors contributed equally to this work. *e-mail: takeuchi@iis.u-tokyo.ac.jp; azettl@berkeley.edu

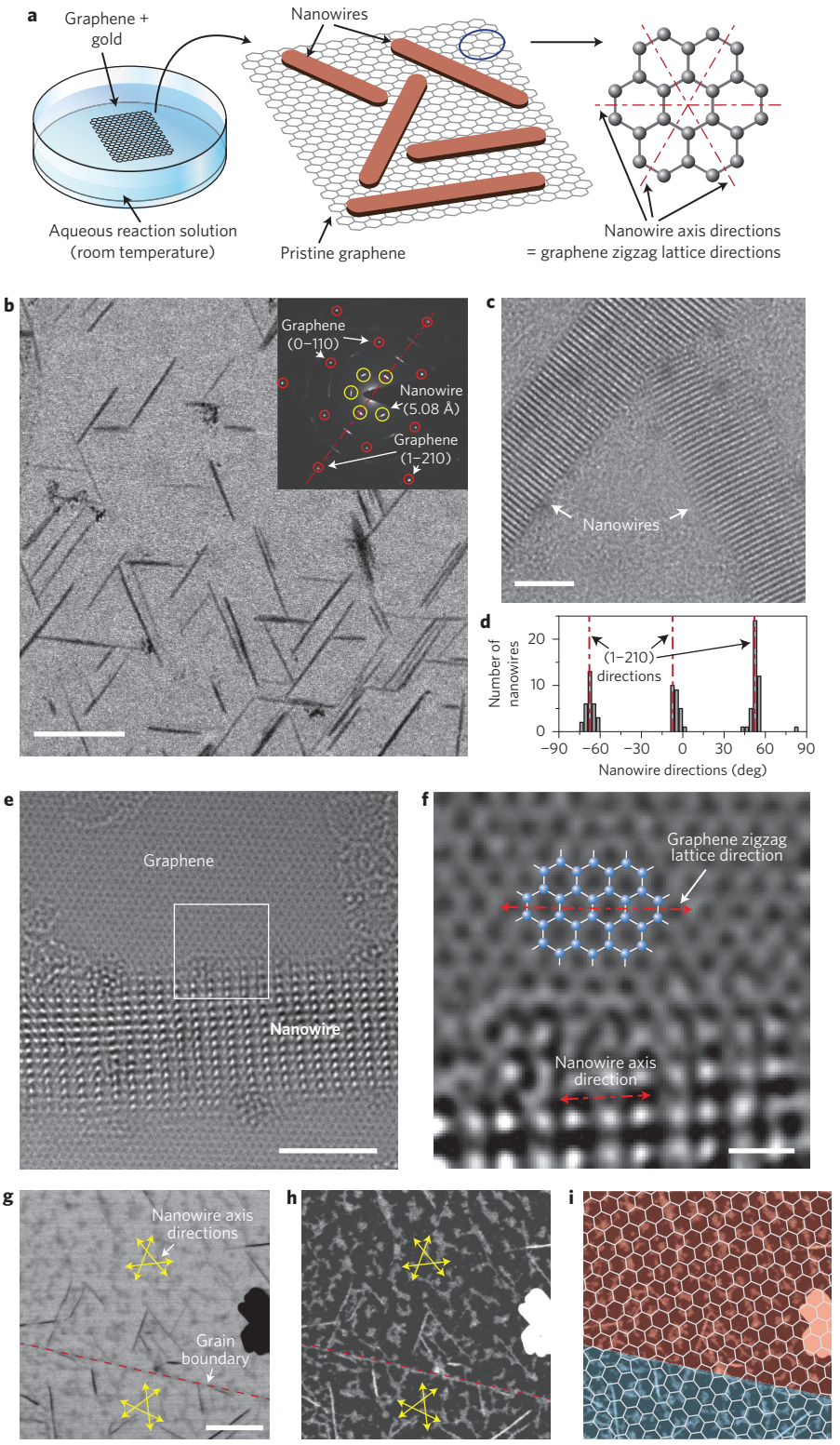

Figure 1 | Directional growth of inorganic nanowires on graphene. a, Schematic of the process. An aqueous-phase reaction at room temperature results in nanowires whose axes are parallel to the zigzag lattice directions of pristine graphene. **b**, TEM image of the synthesized nanowires on graphene. Scale bar, 100 nm. Inset: SAED pattern of the nanowire–graphene sample. The nanowire axes are aligned to the zigzag lattice directions (the (1–210) directions) of graphene. **c**, High-resolution TEM image of the nanowires. Scale bar, 5 nm. **d**, Histogram of the angular distributions of the nanowire axes in **b**. **e**, Atomic-resolution TEM image of a nanowire on graphene. Scale bar, 3 nm. **f**, Enlarged view of box in **e**. Low-pass filtering (cutoff: four pixels) is applied to remove high-frequency noise. The directional alignment of the nanowire axis with the graphene zigzag lattice direction is clearly observed. Scale bar, 0.5 nm. **g–i**, Using the nanowires to image the crystal directions and domain boundaries of polycrystalline graphene. The same specimen area is imaged with TEM (**g**) and SEM (**h**). The graphene lattice directions can be identified using the nanowire axis directions. Scale bar, 100 nm. In **i**, the SEM image (**h**) is shown with an overlay of the pseudo-lattice structures of graphene. The red and blue colour maps represent different domains with relatively tilted lattice directions.

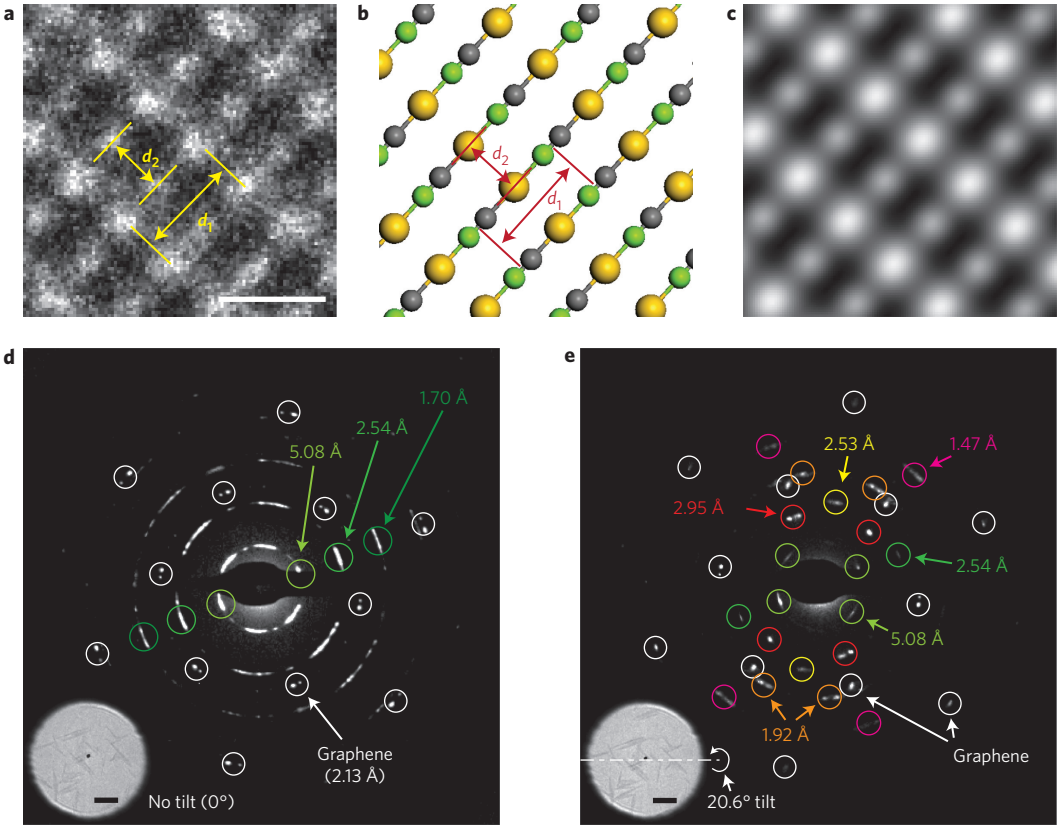

Figure 2 | Atomic-resolution TEM imaging and SAED of the nanowires. a, Atomic-resolution TEM image of the nanowire. The two lattice spacings along (d_1) and perpendicular (d_2) to the nanowire axis direction are measured as 5.08 ± 0.01 Å and 3.00 ± 0.12 Å, respectively. A TEM image of a larger area is provided in Supplementary Fig. 7. Scale bar, 0.5 nm. **b**, Crystal structure of AuCN. The yellow, green and grey spheres represent Au, N and C atoms, respectively. Lattice spacings d_1 and d_2 obtained from the crystal structure are 5.091 Å and 2.937 Å, respectively. **c**, Simulated TEM image from the crystal structure in **b**. The captured TEM image (**a**), crystal structure (**b**) and simulated TEM image (**c**) show good agreement. **d**,**e**, SAED patterns of a nanowire–graphene sample under no tilt (**d**) and 20.6° tilt (**e**). Insets: Sample areas where the SAED patterns are measured. Scale bars (**d**,**e**), 100 nm.

as well as non-graphene C (and a trace amount of H) between all potential constituent elements from the precursor solution (Supplementary Section 'Elemental analysis'). Atomic-resolution TEM imaging (Fig. 2a and Supplementary Fig. 7) and SAED from multiple imaging axes (Fig. 2d,e and Supplementary Fig. 8) allow us to precisely determine the crystal structure. The atomic-resolution TEM images including Fig. 2a directly show unique atomic structures with two orthogonal lattice spacings of 5.08 ± 0.01 Å (d_1) and 3.00 ± 0.12 Å (d_2), which correspond to AuCN's hexagonal crystal[27] (5.091 Å and 2.937 Å). Indeed, AuCN is the sole material candidate that satisfies the observed crystal symmetry and lattice spacings of all the reported inorganic compounds composed of the possible constituent elements (Au, N, C and/or H) classified from the spectroscopic elemental analysis. We further confirmed that the post-simulated TEM image (Fig. 2c) of an AuCN crystal (Fig. 2b) reproduces the unique crystal patterns observed in the experimental TEM images. Most importantly, SAED with multiple imaging axes confirms that the nanowire crystal is AuCN. Owing to the nature of the alignment between the nanowires and graphene, SAED patterns from nanowires with no specimen tilting only display the specific *d*-spacing (5.08 Å) and its high-order peaks from a [100] zone axis (Fig. 2d and Supplementary Fig. 8a). Tilting multiple nanowires within the field of view allows us to investigate a set of SAED peaks from various zone axes and to precisely obtain three-dimensional structural information (Fig. 2e and Supplementary Fig. 8b). All the *d*-spacings measured from the SAED patterns of the nanowires coincide well with those of AuCN (Supplementary Fig. 8c).

The crystal structure also reveals the alignment mechanism between the nanowires and graphene. Because it is well known that lattice matching between two materials causes heteroepitaxial alignment[13,14,24], we compared the in-plane atomic configurations of the nanowires and graphene (Fig. 3a). Along the nanowire axis directions, the unit cell size (d_1) of AuCN (5.08 ± 0.01 Å) coincides well with the length of two carbon hexagons (4.92 Å) along the graphene zigzag directions (lattice mismatch = 3.3 ± 0.2%). In the nanowire width directions, the unit cell sizes ($6d_2$) of AuCN (18.00 ± 0.72 Å) and graphene (19.17 Å) are also matched (lattice mismatch = 6.1 ± 3.8%). Note that the epitaxial alignment of inorganic materials on graphene is successful with a lattice mismatch of ~2.9% (Bi_2Se_3 on graphene[13]), and is possible even with a lattice mismatch of ~28% (MoS_2 on graphene[24]). Thus, in-plane lattice matching is mainly responsible for the epitaxial alignment between the AuCN nanowires and graphene.

We also confirmed that the AuCN nanowires are likely to form directly on pristine surfaces of graphene, although other inorganic materials preferentially attach to dangling bonds such as graphene edges and defects[2,11,13–17]. First, the Raman spectra of graphene before and after nanowire synthesis (Supplementary Fig. 9a,b) maintain very low D peaks, indicating that the graphene is of high quality and measurable defects are not introduced during the nanowire synthesis process. Second, atomic-resolution TEM imaging directly shows the pristine state of the graphene underneath the nanowires. We stripped a nanowire off (Supplementary Fig. 9c,d) and observed a clean graphene lattice without any visible defects (Supplementary Fig. 9e). Third, we synthesized nanowires on

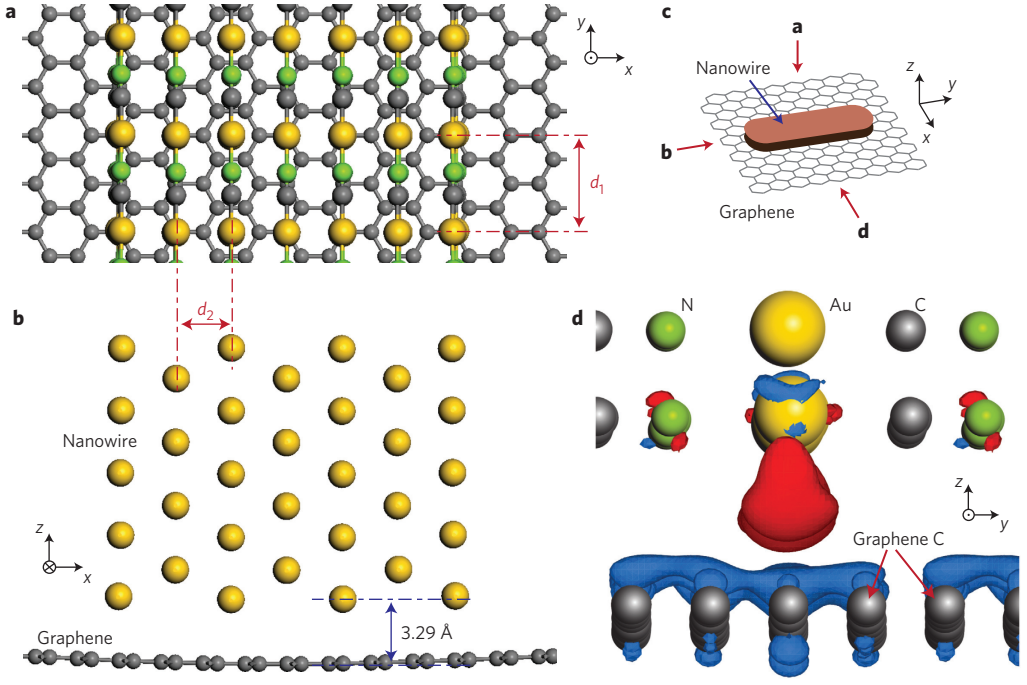

Figure 3 | Interaction between the nanowire and graphene estimated by first-principles calculations. a,**b**, Optimized atomic configuration of the nanowire and graphene estimated by first-principles calculations: plan view from the top (**a**) and side view from the nanowire-axis direction (**b**). **c**, Schematic view of the nanowire and graphene. Red arrows represent the viewing orientations of the panels. **d**, Molecular structures with an overlay of charge density difference isosurfaces at the nanowire–graphene interface. The red and blue charge density difference isosurfaces are contoured at the level of ±0.0004 e Å^{-3}, indicating electron accumulation and depletion, respectively.

sub-monolayer graphene samples consisting of domains that were disconnected from each other. The sub-monolayer graphene, when transferred onto amorphous carbon films of TEM grids, provides three different types of carbon surface for nanowire growth: pristine graphene in the middle of the domains, graphene defects at the edge of the domains, and amorphous carbon (from TEM grids) outside the domains. During synthesis, no nanowire is formed on amorphous carbon surfaces and the nanowire density is uniform throughout the graphene domains and edges (Supplementary Fig. 9f–h). These results imply that the nanowires grow preferentially on pristine graphene surfaces (not on graphene defects) and do not perturb the crystal structure of the graphene. Moreover, the third experiment (Supplementary Fig. 9f–h) indicates that graphene is a unique substrate promoting the formation of uncommon inorganic crystals. As also shown by the synthesis of new organic crystals on graphene[5,7,8], this result suggests the possibility of using graphene as a template for advanced nanostructuring of inorganic materials.

The nanowire growth on pristine graphene suggests that the interaction between the two materials is unusual for inorganic materials. Owing to the chemical inertness of graphene, the only way previously shown to synthesize inorganic structures directly on pristine graphene has been vapour-phase deposition[12–14,23–25], which is mainly performed at high temperatures (400–900 °C). However, the reaction in this study occurs in the aqueous phase at room temperature, which suggests that the interaction between the nanowires and pristine graphene provides a sufficient driving force for assembly without high energy. Thus, we investigated the interaction between the nanowires and graphene using first-principles calculations (Supplementary Methods). In the optimized atomic configuration (Fig. 3a,b), both AuCN's hexagonal crystal and graphene's sp^2 carbon structures remain intact, and their interlayer distance (3.29 Å) is almost the same as the interlayer distance (3.31 Å) between Au(111) and graphene[28]. The parallel atomic structure at the interface (Fig. 3b,d) suggests that Au atoms, whose covalent radius (1.3 Å) is significantly larger than those of C and N (0.7 Å), contribute predominantly to the interaction between the nanowire and graphene. The major binding contribution of Au atoms is also confirmed in the charge density difference (Fig. 3d), where transferred electrons are localized only near Au atoms. However, the interaction between graphene and Au atoms in AuCN has unique characteristics that differ from the common physical interaction between graphene and Au(111). The calculated binding energy of AuCN on graphene is 181 meV/Au, significantly greater than the 80 meV/Au for the binding energy between Au (111) and graphene via electrostatic interaction[28]. The charge density difference (Fig. 3d) shows that the π orbitals of graphene donate electrons to Au atoms in AuCN. These characteristics support the notion that the nanowire– graphene interaction is mainly attributed to electron transfer between a transition metal (Au) and cyclic π systems. This type of interaction, previously studied in organometallic chemistry, differs from the relatively weak physisorption[2,14,28] (either electrostatic or van der Waals interaction) that is commonly observed at interfaces between inorganic crystals and graphene. We note that the organometallic π interaction with graphene has been found with only a few inorganic materials[29], which are not even crystals but molecules. The unique π interaction is presumably responsible for the spontaneous binding between the nanowires and graphene, and it also offers the possibility of synthesizing various inorganic materials on pristine graphene without disturbing sp^2 carbon networks[2,29].

The as-prepared nanowires allowed us to fabricate nanostructures with controlled crystallographic orientations (Fig. 4a). First, graphene nanoribbons with zigzag-edged directions (which can be important components in spintronic devices[30]) were fabricated using the synthesized nanowires as an etching mask. The nanowire-covered graphene was selectively protected from O_2 plasma etching (Fig. 4b), and the nanowires were then removed with a

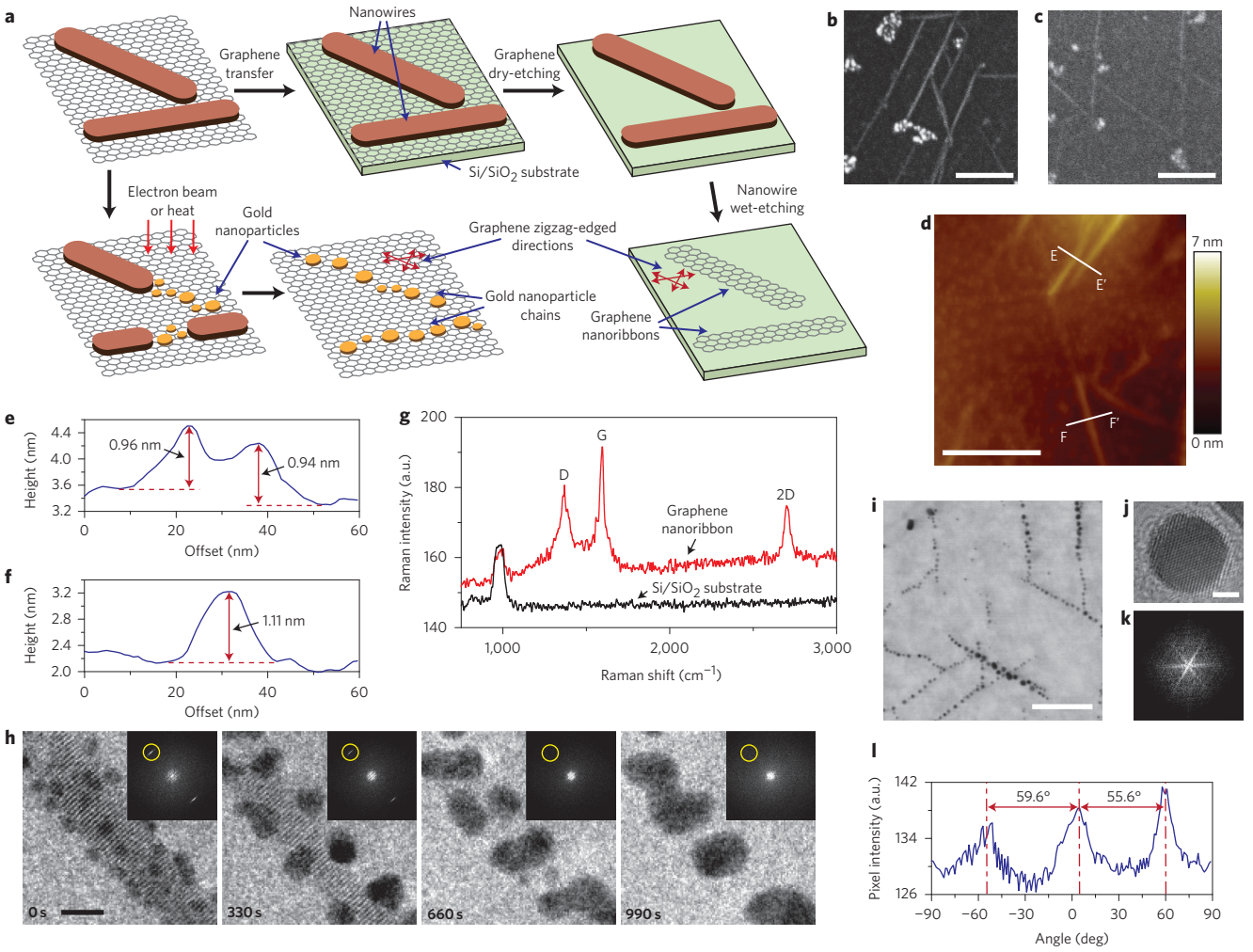

Figure 4 | Fabrication of crystallographically aligned nanostructures. a, Fabrication process for the graphene nanoribbons and gold nanoparticle chains based on the nanowires aligned on graphene. **b**,**c**, SEM images of the nanowires after graphene dry-etching (**b**) and the fabricated graphene nanoribbons (**c**), which are aligned with the zigzag lattice directions. Scale bars, 100 nm. **d**, AFM image of the graphene nanoribbons. Scale bar, 100 nm. **e**,**f**, Height profiles of the sample along E–E′ (**e**) and F–F′ (**f**) in **d**. **g**, Raman spectrum of the fabricated graphene nanoribbons (red line). The negative control signal (black line) is measured from a position where the graphene is fully etched out in the same sample. **h**, A series of TEM images from Supplementary Movie 1 showing the nanowire decomposition process to gold nanoparticle chains under electron-beam irradiation. Insets: Fourier transforms of the TEM images. Scale bar, 5 nm. **i**, Gold nanoparticle chains formed by thermal decomposition of nanowires. Scale bar, 100 nm. **j**, High-resolution TEM image of a gold nanoparticle in the chain. Scale bar, 2 nm. **k**, Fourier transform of **i**. The directions of the bright lines are orthogonal to the axis directions of the gold nanoparticle chains. **l**, Radial pixel intensities of **k**, averaged along a line from the centre at different angles. The directional alignment of the gold nanoparticle chains is shown with inter-peak angles of ~60°.

NaOH solution without damaging the graphene (Fig. 4c and Supplementary Fig. 10). Because the nanowires are conformally attached on the graphene and their widths can be controlled to within less than 10 nm, the present method readily enables us to fabricate graphene nanoribbons with sub-10 nm widths. The AFM image in Fig. 4d and its height profiles (Fig. 4e,f) indicate that the widths of the fabricated graphene nanoribbons are near 10 nm, with the tip-size effect taken into account. In addition, the thickness of the fabricated graphene nanoribbon is ~1 nm, which is consistent with the reported thickness[31] of single-layered graphene on SiO_2. The Raman spectrum (Fig. 4g) also indicates that the graphene nanoribbons are fabricated successfully. The intensity ratio of the D and G bands (I_D/I_G), a common measure to evaluate the quality of carbon materials, is ~0.67, which is advanced for graphene nanoribbons produced by top-down fabrication. Overall, the AFM and Raman data indicate that the fabricated graphene nanoribbons are of reasonable quality (in particular the edge smoothness) compared to previously available graphene nanoribbons[31]. The crucial point in this fabrication process is that the directional alignment of the nanowires allows us to selectively fabricate graphene nanoribbons in zigzag-edged directions. Note that it has been difficult to fabricate graphene nanoribbons with zigzag-edged directions and only a few previous studies[32] have achieved it so far.

As the second example of crystallographically aligned nanostructures we fabricated gold nanoparticle chains aligned to the crystal directions of graphene substrates by decomposing the nanowires to gold nanoparticles (Fig. 4a). The electron beam in TEM was used to decompose the synthesized nanowires on graphene (Supplementary Movie 1 and Fig. 4h). Gold nanoparticles (dark dots) grow near the nanowire and finally replace the entire nanowire (Supplementary Fig. 11). The application of heat (200 °C, 30 min) can also decompose the nanowires to gold nanoparticles (Fig. 4i,j). Because the nanowire arrangement determines the position of the gold nanoparticle, the gold nanoparticle chains are naturally aligned along the zigzag lattice directions of the graphene substrate (Fig. 4k,l). These gold nanoparticle chains are in the

optimal dimension for near-field plasmon coupling[33], which can propagate and/or enhance the electromagnetic waves of applied light along the chain axes. Thus, light with a particular wavelength and polarization will interact strongly along specific crystal directions of the graphene. This phenomenon suggests potential applications in optical measurements of graphene crystal directions and plasmonic sensing platforms.

In summary, we have presented the self-organized growth of inorganic AuCN nanowires that are readily aligned to the zigzag lattice directions of single-layered pristine graphene. This direct alignment can be utilized to extract and control crystallographic information about nanostructures, thus enabling us to fabricate graphene nanoribbons with zigzag-edged directions. The synthetic method we have introduced demonstrates the possibility of using graphene as a template for advanced classes of inorganic nanomaterials, even with wet chemistry. Furthermore, the unique interaction found in this study may provide a new direction for the fabrication of graphene–inorganic heterostructures with intrinsic interface properties.

Received 14 May 2014; accepted 9 February 2015;
published online 23 March 2015

References

1. Geim, A. K. & Grigorieva, I. V. Van der Waals heterostructures. *Nature* **499,** 419–425 (2013).
2. Georgakilas, V. *et al.* Functionalization of graphene: covalent and non-covalent approaches, derivatives and applications. *Chem. Rev.* **112,** 6156–6214 (2012).
3. Huang, X., Qi, X., Boey, F. & Zhang, H. Graphene-based composites. *Chem. Soc. Rev.* **41,** 666–686 (2012).
4. Barth, J. V., Costantini, G. & Kern, K. Engineering atomic and molecular nanostructures at surfaces. *Nature* **437,** 671–679 (2005).
5. Hong, G. *et al.* Recent progress in organic molecule/graphene interfaces. *Nano Today* **8,** 388–402 (2013).
6. Kim, D. W., Kim, Y. H., Jeong, H. S. & Jung, H-T. Direct visualization of large-area graphene domains and boundaries by optical birefringency. *Nature Nanotech.* **7,** 29–34 (2012).
7. Garnica, M. *et al.* Long-range magnetic order in a purely organic 2D layer adsorbed on epitaxial graphene. *Nature Phys.* **9,** 368–374 (2013).
8. Colson, J. W. *et al.* Oriented 2D covalent organic framework thin films on single-layer graphene. *Science* **332,** 228–231 (2011).
9. Zhang, F. *et al.* Epitaxial growth of peptide nanofilaments on inorganic surfaces: effects of interfacial hydrophobicity/hydrophilicity. *Angew. Chem. Int. Ed.* **45,** 3611–3613 (2006).
10. Fukushima, T. *et al.* Molecular ordering of organic molten salts triggered by single-walled carbon nanotubes. *Science* **300,** 2072–2074 (2003).
11. Chung, K., Lee, C-H. & Yi, G-C. Transferable GaN layers grown on ZnO-coated graphene layers for optoelectronic devices. *Science* **330,** 655–657 (2010).
12. Addou, R., Dahal, A. & Batzill, M. Growth of a two-dimensional dielectric monolayer on quasi-freestanding graphene. *Nature Nanotech.* **8,** 41–45 (2013).
13. Dang, W., Peng, H., Li, H., Wang, P. & Liu, Z. Epitaxial heterostructures of ultrathin topological insulator nanoplate and graphene. *Nano Lett* **10,** 2870–2876 (2010).
14. Hong, Y. J. *et al.* Van der Waals epitaxial double heterostructure: InAs/single-layer graphene/InAs. *Adv. Mater.* **25,** 6847–6853 (2013).
15. Wang, X., Tabakman, S. M. & Dai, H. Atomic layer deposition of metal oxides on pristine and functionalized graphene. *J. Am. Chem. Soc.* **130,** 8152–8153 (2008).
16. Alaboson, J. M. P. *et al.* Templating sub-10 nm atomic layer deposited oxide nanostructures on graphene via one-dimensional organic self-assembled monolayers. *Nano Lett.* **13,** 5763–5770 (2013).
17. Kim, K. *et al.* Selective metal deposition at graphene line defects by atomic layer deposition. *Nature Commun.* **5,** 4781 (2014).
18. Liang, Y. *et al.* Co_3O_4 nanocrystals on graphene as a synergistic catalyst for oxygen reduction reaction. *Nature Mater.* **10,** 780–786 (2011).
19. Si, Y. & Samulski, E. T. Exfoliated graphene separated by platinum nanoparticles. *Chem. Mater.* **20,** 6792–6797 (2008).
20. Lightcap, I. V., Kosel, T. H. & Kamat, P. V. Anchoring semiconductor and metal nanoparticles on a two-dimensional catalyst mat. Storing and shuttling electrons with reduced graphene oxide. *Nano Lett.* **10,** 577–583 (2010).
21. Choi, D. *et al.* Fully rollable transparent nanogenerators based on graphene electrodes. *Adv. Mater.* **22,** 2187–2192 (2010).
22. Huang, X. *et al.* Reduced graphene oxide-templated photochemical synthesis and *in situ* assembly of Au nanodots to orderly patterned Au nanodot chains. *Small* **6,** 513–516 (2010).
23. Kumar, B. *et al.* Controlled growth of semiconducting nanowire, nanowall, and hybrid nanostructures on graphene for piezoelectric nanogenerators. *ACS Nano* **5,** 4197–4204 (2011).
24. Shi, Y. *et al.* Van der Waals epitaxy of MoS_2 layers using graphene as growth templates. *Nano Lett.* **12,** 2784–2791 (2012).
25. Zhou, H. *et al.* The transformation of a gold film on few-layer graphene to produce either hexagonal or triangular nanoparticles during annealing. *Carbon* **52,** 379–387 (2013).
26. Kim, K. *et al.* Grain boundary mapping in polycrystalline graphene. *ACS Nano* **5,** 2142–2146 (2011).
27. Hibble, S. J., Hannon, A. C. & Cheyne, S. M. Structure of AuCN determined from total neutron diffraction. *Inorg. Chem.* **42,** 4724–4730 (2003).
28. Giovannetti, G. *et al.* Doping graphene with metal contacts. *Phys. Rev. Lett.* **101,** 026803 (2008).
29. Sarkar, S. *et al.* Organometallic hexahapto functionalization of single layer graphene as a route to high mobility graphene devices. *Adv. Mater.* **25,** 1131–1136 (2013).
30. Son, Y-W., Cohen, M. L. & Louie, S. G. Half-metallic graphene nanoribbons. *Nature* **444,** 347–349 (2006).
31. Jiao, L., Zhang, L., Wang, X., Diankov, G. & Dai, H. Narrow graphene nanoribbons from carbon nanotubes. *Nature* **458,** 877–880 (2009).
32. Shi, Z. *et al.* Patterning graphene with zigzag edges by self-aligned anisotropic etching. *Adv. Mater.* **23,** 3061–3065 (2011).
33. Halas, N. J., Lal, S., Chang, W. S., Link, S. & Nordlander, P. Plasmons in strongly coupled metallic nanostructures. *Chem. Rev.* **111,** 3913–3961 (2011).

Acknowledgements

The authors thank A.P. Alivisatos, H. Fujita, Y. Arakawa, B.J. Kim, L. Yang, J. Moon, Y. Ota, H. Suh, J. Kwon and J. Min for helpful discussions. The authors also thank J. Kim and Y. Mizutani for the AFM analysis, S. Mori and M. Onuki for technical support and A. Sato for help with graphic illustrations. This work was mainly supported by the Takeuchi Biohybrid Innovation Project, Exploratory Research for Advanced Technology (ERATO), Japan Science and Technology (JST). A.Z. and K.K. acknowledge support from the Director, Office of Energy Research, Materials Sciences and Engineering Division, of the US Department of Energy (DE-AC02-05CH11231) and from the Office of Naval Research (MURI grant N00014-09-1066). K.K. also acknowledges support from the Basic Science Research Program through the National Research Foundation of Korea (NRF) funded by the Ministry of Education (NRF-2014R1A1A2058178). D.A.W. and J.P. acknowledge support from the Harvard MRSEC (DMR-0820484) and Amore-Pacific. H.L. and J.K. acknowledge support from the Basic Science Research Program through the National Research Foundation of Korea, funded by the Ministry of Science, ICT & Future Planning (NRF-2015R1A1A1001583) and also acknowledge support from KISTI under the Supercomputing Applications Support Program (KSC-2013-C3-034). H.Y.J. acknowledges support from the 2012 Research Fund (1.120032.01) of UNIST.

Author contributions

W.C.L., K.K. and J.P. conceived the design of the study. S.T., A.Z. and D.A.W. supervised the project. K.K. and J.P. initially discovered the nanowire synthesis phenomenon. W.C.L., K.K., J.P. and H.Y.J. performed all experiments. J.K. and H.L. performed first-principles calculations. W.C.L., K.K., J.P., H.L., D.A.W., A.Z. and S.T. wrote the manuscript. All authors discussed the results and commented on the manuscript.

Additional information

Supplementary information is available in the online version of the paper. Reprints and permissions information is available online at www.nature.com/reprints. Correspondence and requests for materials should be addressed to A.Z. and S.T.

Competing financial interests

The authors declare no competing financial interests.

nature nanotechnology

SUPPLEMENTARY INFORMATION

DOI: 10.1038/NNANO.2015.36

Graphene-templated directional growth of an inorganic nanowire

Won Chul Lee†, Kwanpyo Kim†, Jungwon Park†, Jahyun Koo, Hu Young Jeong, Hoonkyung Lee, David A. Weitz, Alex Zettl*, and Shoji Takeuchi*

†These authors equally contributed to this work.

*To whom correspondence should be addressed.

Supplementary Text

Elemental analysis We analyse the nanowire samples using energy dispersive x-ray spectroscopy (EDX) and electron energy loss spectroscopy (EELS). In this elemental analysis, we focus on the elements of C, N, O, S, (H), and Au, which the precursor solution contains. The EDX spectra with/without the nanowires (Supplementary Fig. 5a, b) indicate the presence of Au within the nanowires. We also confirm that Au is localized in the nanowires using EDX chemical mapping (Supplementary Fig. 5c, d). Using EDX for identifying other light elements is not appropriate because e-beam irradiation decomposes the nanowire material (Fig. 4h–j and Supplementary Video 1) and light elements (C, H, O, and S) are lost during the long measurement time of EDX (in our case, 30 sec with an electron voltage of 100 kV). EELS has better sensitivity for observation of light elements and can reduce the measurement time (in our case, 0.2 sec × 5 times with an electron voltage of 80 kV), thus allows us to further identify those elements from our nanowires. The EELS spectra with/without the nanowires (Supplementary Fig. 6a–d) show the presence of N within the nanowires in the repeated measurements. The peaks for O and S from the precursor solution are not present in the nanowires. We additionally confirm that N is localized in the nanowires using energy-

filtered TEM imaging at N K-edge (Supplementary Fig. 6e, f). Taken together, our EDX and EELS results indicate that the nanowires contain Au and N with the possible presence of C and/or H.

In addition, characteristic features of the measured EELS carbon peaks should be noted. The energy loss region at the C 1s (K edge) consists of two peaks – a sharp peak near 285 eV due to excitation to π^* states and a broad peak over 290 eV due to excitation to σ^* states[34]. While the sample areas without nanowires (Supplementary Fig. 6b, c) show typical EELS spectra of graphene, the EELS carbon spectrum from the nanowires (Supplementary Fig. 6a) shows different characteristics; the height ratio of the π^* peak to the σ^* peak is larger than that of graphene. This feature suggests that the nanowires have the increased number of π-bonded electrons compared to graphene (sp^2 bonded carbons), thus indicating the possible presence of sp^1 bonded carbons in the nanowires. This observation is consistent with the sp^1 electronic state of carbon atoms in AuCN.

Supplementary Methods

Graphene preparation Graphene is synthesized by chemical vapour deposition (CVD) on 25 μm thick copper foil (99.8 %, Alfa Aesar, Ward Hill, MA). The copper foil is inserted into a quartz tube and heated to 1,000 °C under a H_2 flow of 10 sccm at 150 mTorr. After annealing for 30 min, a gas mixture of 25 sccm CH_4 and 10 sccm H_2 at 520 mTorr is introduced for 20 min to synthesize graphene. Finally, fast cooling to room temperature with a CH_4 flow of 20 sccm under a pressure of 330 mTorr is performed. Graphene samples purchased from Graphene Platform, Inc. are also tested. For the nanowire synthesis experiments shown in Supplementary Fig. 9f-h, sub-monolayer graphene samples are used. The 25 sccm CH_4 flow is introduced only for 1 min during graphene growth.

Au nanoparticle preparation Two types of Au nanoparticles are used in this study: spherical Au nanoparticles (diameter: 8 nm) dispersed in toluene and Au nanorods (diameter: 25 nm, length: 73

nm, purchased from Nanopartz Inc.) dispersed in ethanol. The spherical Au nanoparticles are prepared by the following synthetic method, as previously reported[35], with modifications. Required chemicals: Gold chloride ($AuCl_3$, 99 %, Aldrich), didodecyldimethylammonium bromide (DDAB, Fluka), sodium borohydride ($NaBH_4$, 99.99 %, Aldrich), and dodecanethiol (DDTh, > 98 %, Aldrich) are purchased and used without further purification. 51 mg of gold chloride and 0.173 g of DDAB are dissolved by sonication in 15 mL toluene. A total of 54 μL of 9.4 M $NaBH_4$ aqueous solution is added dropwise to the reaction flask while stirring the solution at room temperature. Red-coloured gold colloids form after 20 min. A 1.5 mL aliquot of DDTh is added to the gold colloids for ligand exchange. The gold nanocrystals are then precipitated with ethanol, vacuum-dried, and re-dissolved into 45 mL of toluene. Another 4.5 mL of DDTh is added, and the solution is heated under reflux for 12 hour. Gold nanocrystals are precipitated with acetone and re-dispersed in toluene. This solution is further filtered with qualitative grade filter paper to remove any aggregated gold colloids. The gold nanocrystals are re-dispersed in 5 mL toluene and maintain colloidal stability for several months. The gold nanoparticles are diluted with toluene to desired concentration for nanowire synthesis (for typical experiments, a 1/10 dilution factor is used).

Nanowire synthesis The nanowire synthesis on graphene is performed with different types of gold precursors: (i) spherical gold nanoparticles, (ii) gold nanorods, and (iii) a gold grid mesh (Supplementary Fig. 1). Most of the reaction parameters are maintained across the different methods, with the exception of the choice of gold precursors. The nanowire synthesis using Au nanoparticles begins with transferring graphene to Quantifoil holey carbon TEM grids using a direct transfer method[36]. In brief, the Quantifoil TEM grid is placed onto a graphene-covered copper foil with the Quantifoil carbon film side facing the graphene. Then 2.5 μl of isopropyl alcohol (IPA) is dropped onto the sample to wet the interface, and the sample is dried at 85 °C on a hot plate for 15 min to promote adhesion between the Quantifoil carbon film and the graphene. The grid is floated on an

aqueous solution of 113 mM ammonium persulfate, $(NH_4)_2S_2O_8$, to etch the underlying copper foil and rinsed several times by floating the graphene transferred grid on deionized water. After the graphene transfer is complete, Au nanoparticles (either spherical nanoparticles or nanorods) dispersed in organic solvents are dropped and dried on the grids. Then, the grids are floated on an aqueous solution of 250 mM ammonium persulfate, $(NH_4)_2S_2O_8$, for 17 hours to initiate nanowire growth on the graphene and rinsed by transferring the grids to deionized water multiple times. In the nanowire synthesis process using a grid mesh as an Au precursor, a graphene-covered copper foil is partially cut before transferring the graphene to TEM grids, such that the Au grid mesh is exposed to the reaction solution during incubation. As a result, the density of the nanowires formed on graphene is higher near the exposed Au grid mesh.

Electron microscopy Conventional TEM images are captured using a JEOL JEM 2010F TEM operated at 200 kV and a JEOL JEM 2100 TEM operated at 200 kV. Low-resolution TEM and SEM images are captured using a Hitachi SU8000 FE-SEM operated at 30 kV.

Aberration-corrected TEM Aberration-corrected TEM images are captured with a TEAM 0.5 microscope at the National Center for Electron Microscopy at Lawrence Berkeley National Laboratory. The microscope is equipped with an image Cs aberration corrector and a monochromator. The images are acquired at 80 kV, and the Cs coefficient is set to approximately -10 μm. The TEM images are taken at an over-focus of 10 nm, which allows an optimal imaging condition with bright atom contrast.

AFM A Park Systems NX-10 AFM with an Olympus silicon microcantilever (AC160TS-C3, tip radius: 7 nm) is operated under ambient conditions.

Spectroscopy EDX point analysis is performed using a Noran Voyager III M3100 connected to a Hitachi HF-2000 FE-TEM (operation voltage: 100 kV). EDX elemental mapping is performed with a JEOL 2100F (operated at 200 kV), equipped with a field emission gun and a probe C_s corrector. EELS point spectra and EELS mapping at N K edge are acquired with a FEI Titan Cube G2 60-300 operated at 80 kV. Gatan GIF Quantum 965 is used as an EELS detector. Raman spectroscopy is performed using a Jasco NRS-5100 laser Raman spectrometer (excitation wavelength: 532 nm).

First-principles calculations The calculations for AuCN nanowires on graphene are performed using density functional theory (DFT) implemented in the Vienna Ab-initio Simulation Package (VASP) with a projector-augmented-wave (PAW) method. For the exchange correlation energy functional, the local density approximation (LDA) is employed, and the kinetic energy cutoff is taken to be 400 eV. The AuCN nanowire is obtained through minimization of the total energy, starting with (100) AuCN with a width of 1.7 nm and a height of 1.3 nm. In the initial structure for investigating the interaction between the nanowire and graphene, the AuCN nanowire is placed on single-layer graphene at a distance of ~3 Å. Geometry optimization of the structures is carried out until the Hellmann–Feynman force acting on each atom is smaller than 0.01 eV/Å. The plan-view of the unit cell is illustrated in Fig. 3a. The first Brillouin zone integration is performed using the Monkhorst–Pack scheme, and 10×4×1 k-point sampling for the nanowire is used. The binding energy between the nanowire and graphene is calculated by subtracting energies of the isolated nanowire and graphene from the total energy of the nanowire-graphene complex.

TEM image simulation from the crystal structure The TEM image simulations are performed using MacTempas and CrystalKit. The imaging acquisition conditions including a defocus value of 12 nm are used for the simulations of the AuCN crystal of 2 nm in thickness in the imaging crystal axis.

Graphene nanoribbon fabrication Graphene decorated with the nanowires is prepared on a TEM grid as described above. The graphene sample is then placed on a silicon wafer through the following method. First, a silicon wafer with thermal oxide is cleaned using oxygen plasma. The TEM grid is placed onto the wafer with the graphene side facing up. Then, 2.5 μL of IPA is dropped onto the sample to wet the interface between the backside of graphene and the silicon substrate. While the sample is dried at 85 °C on a hot plate for 1 hour, capillary forces generated by the evaporation of IPA promotes adhesion between the backside of the graphene and the silicon substrate. This process prepares the graphene to be sandwiched between the wafer and nanowires. The dry etching of graphene is performed using a Samco RIE-10 NR system with an oxygen gas flow rate of 10 sccm and a power of 30 W for 6.5 sec. Finally, the nanowires are etched off with a 0.42 M NaOH solution for 1 hour without damaging the graphene nanoribbons (Supplementary Fig. 10).

Supplementary Video legend

Supplementary Video 1. In-situ TEM video showing the nanowire decomposition to Au nanoparticle chains under e-beam irradiation with a 200 kV acceleration voltage and 106 μA beam current. The video (total area: 90.3 nm by 90.3 nm) has been accelerated by a factor of 50, displaying 5 fps (frames per second) while real time corresponds to 0.1 fps.

References in Supplementary Information

34. Robertson, J. Diamond-like amorphous carbon. *Mat. Sci. Eng. R* **37**, 129-281 (2002).
35. Lin, X. M., Jaeger, H. M., Sorensen, C. M. & Klabunde, K. J. Formation of long-range-ordered nanocrystal superlattices on silicon nitride substrates. *J. Phys. Chem. B* **105**, 3353-3357 (2001).
36. Regan, W. *et al.* A direct transfer of layer-area graphene. *Appl. Phys. Lett.* **96**, 113102 (2010).

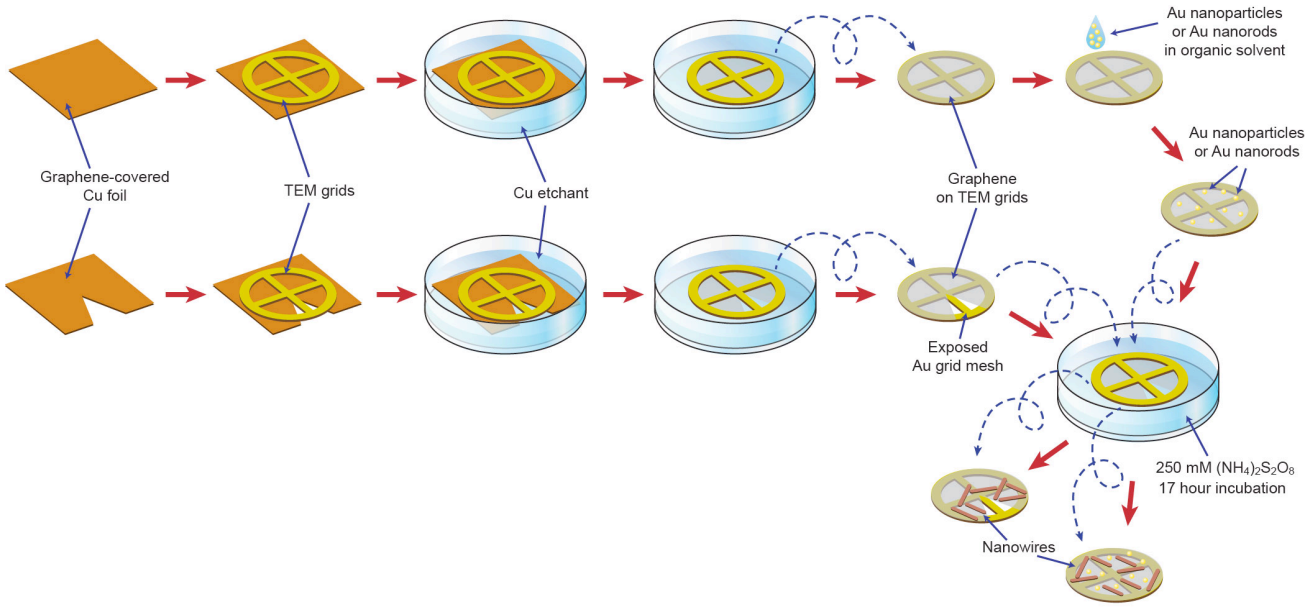

Supplementary Figure 1. Graphene transfer and nanowire synthesis. Three types of gold precursors are used for the nanowire synthesis in this study, with the majority of the remaining reaction parameters maintained constant. The nanowire synthesis using Au nanoparticles/nanorods (upper part in this figure) begins with transferring CVD-synthesized graphene to TEM grids. Then, Au nanoparticles/nanorods dispersed in organic solvents are dropped on the grids and dried. The nanowires are synthesized on graphene by floating the grids on an aqueous solution of 250 mM ammonium persulfate, $(NH_4)_2S_2O_8$, for 17 hours. In the nanowire synthesis using a grid mesh as an Au source (lower part in this figure), a graphene-covered copper foil is partially cut before the graphene is transferred to TEM grids. Then, without dropping the nanoparticles/nanorods, the grid is floated on the reaction solution for the nanowire synthesis. The Au grid mesh is partially exposed to the reaction solution during the incubation.

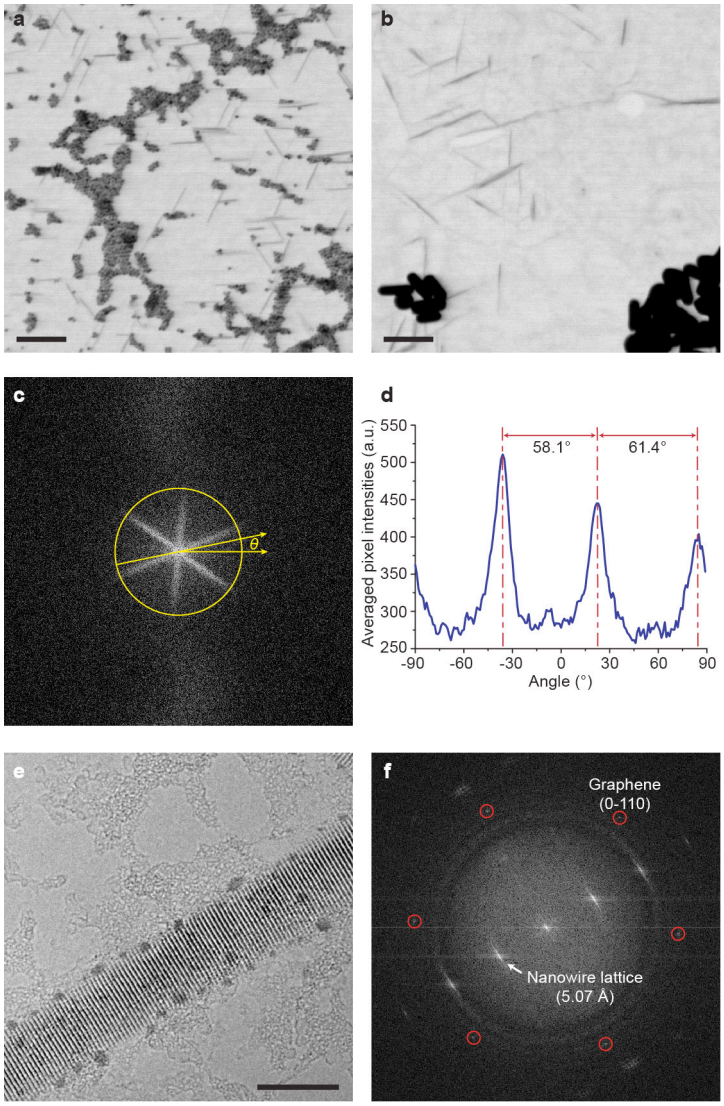

Supplementary Figure 2. TEM images of the nanowires. a–b, TEM images of the nanowires synthesized from various types of gold sources. Spherical Au nanoparticles (**a**), Au nanorods (**b**), or Au of TEM grids (Fig. 1b) are used in the nanowire synthesis. The scale bars represent 100 nm. **c**, Fourier transform of Fig. 1b. The directions of three bright lines are orthogonal to the directions of nanowire axes. **d**, Radial pixel intensities of **c** averaged along the line from the centre at different angles. The three peaks represent the nanowire alignment. **e**, High-resolution TEM image of a nanowire. The scale bar represents 10 nm. **f**, Fourier transform of **e**.

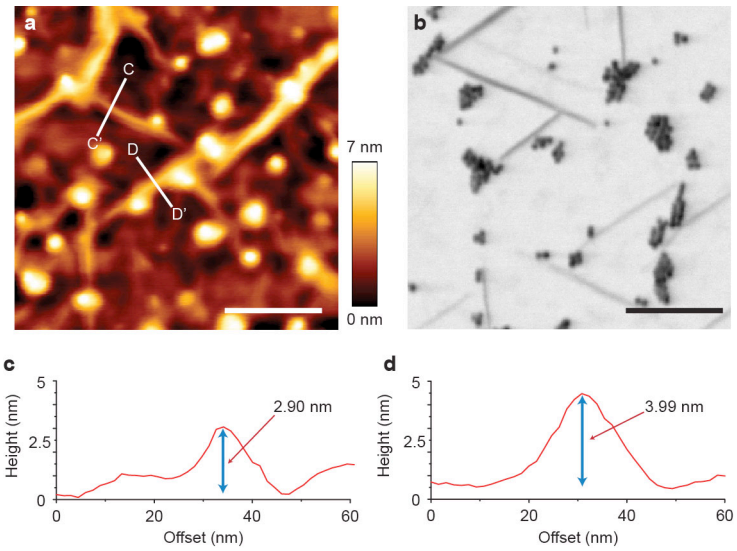

Supplementary Figure 3. AFM (Atomic force microscopy) analysis of the nanowires. a, AFM image of the nanowires synthesized from Au nanoparticles. The bright dots show Au nanoparticle clusters, and the bright lines are the synthesized nanowires. The scale bar represents 100 nm. **b**, TEM image of the same sample as **a**. The scale bar represents 100 nm. **c**–**d**, Height profiles of the sample along the C–C' (**c**) and D–D' (**d**) lines in **a**. The nanowire thickness is measured as 3.29 ± 0.47 nm from 7 repeated measurements.

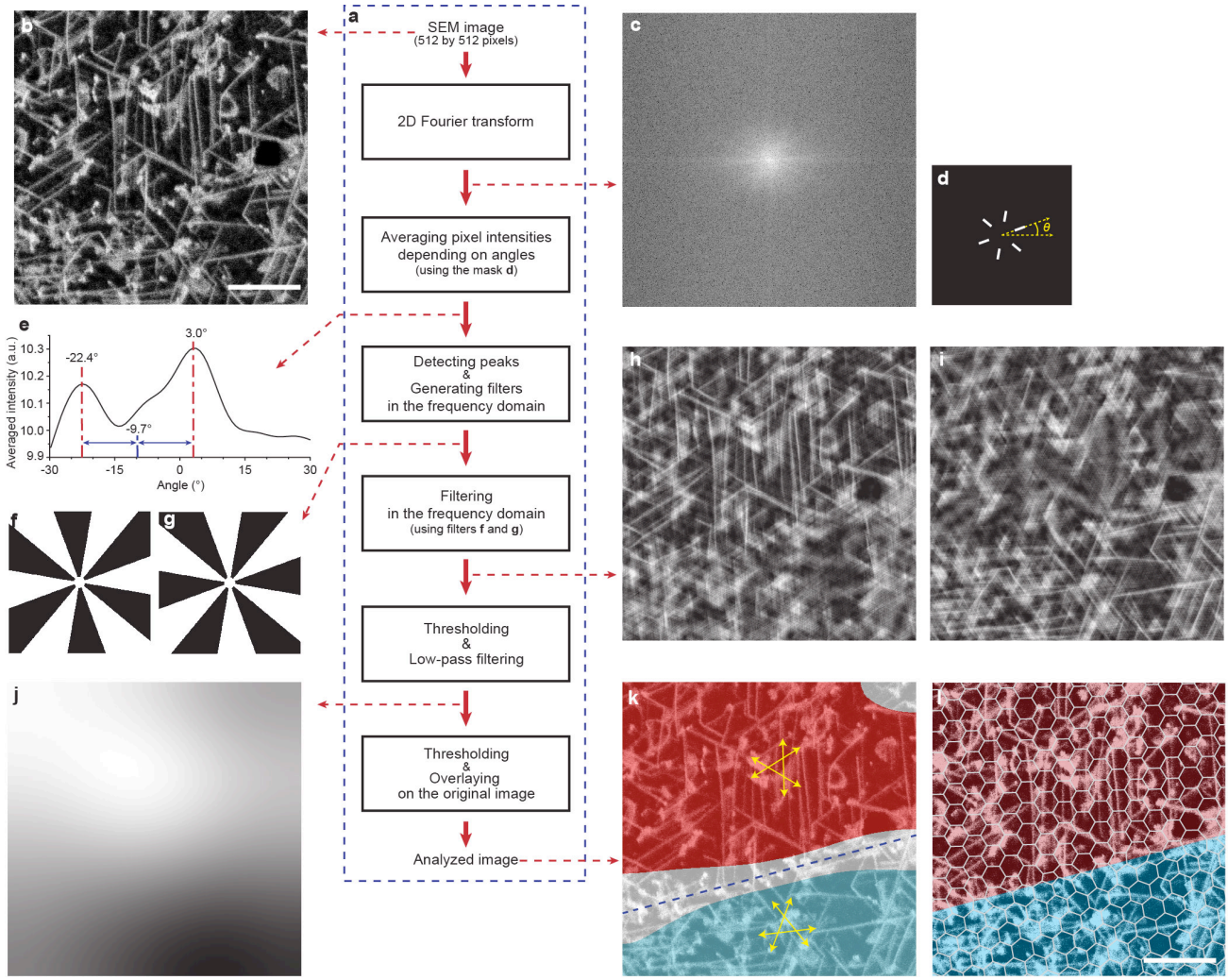

Supplementary Figure 4. Automated image processing for the SEM-based visualization of crystal directions and grain boundaries in polycrystalline graphene. **a**, Process chart for the automated image processing. **b**, Initial SEM image of the nanowires on polycrystalline graphene. The scale bar represents 100 nm. **c**, Fourier transform of **b**. **d**, Mask image for averaging the pixel intensities of **c**. **e**, Averaged pixel intensities of **c** depending on the angles, θ. The two peaks present two graphene grains whose crystal directions are tilted relative to each other. **f-g**, Frequency-domain filters for the image separation of the two graphene grains. **h-i**, Filtered images of **b** using **f** and **g**. The nanowires on the bottom part and the upper part of the original image (**b**) are selectively filtered out in **h** and **i**, respectively. **j**, Black and white map representing the difference in nanowire densities in **h** and **i**. **k-l**, Initial SEM image (**b**) with overlays of colour maps calculated from the automated image processing (**k**) and manually obtained (**l**). The red and blue colour maps represent different grains tilted relative to each other. The spatial resolution of the automated image processing is approximately 100 nm for this experimental condition.

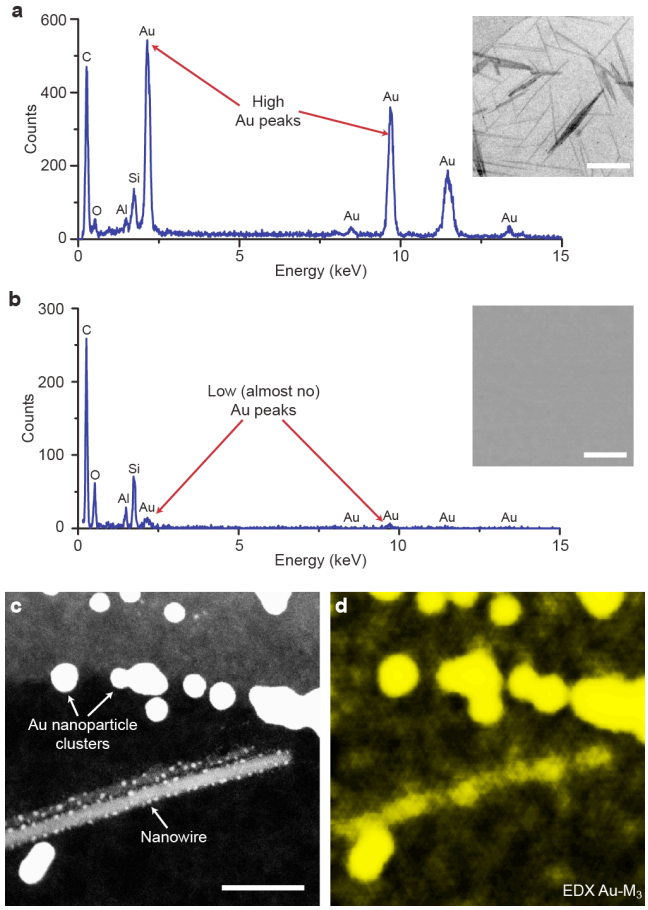

Supplementary Figure 5. Energy-dispersive X-ray spectroscopic (EDX) analysis of the nanowires. a–b, EDX spectra of the nanowires on graphene (**a**) and graphene substrate without the nanowires (**b**). The spectra are measured from the entire areas of the insets. The scale bars indicate 100 nm. The peaks indicate the presence of Au within the nanowires. **c–d**, EDX chemical mapping of the sample. The ADF TEM image (**c**) and the gold chemical map (**d**) are displayed. The scale bar indicates 25 nm.

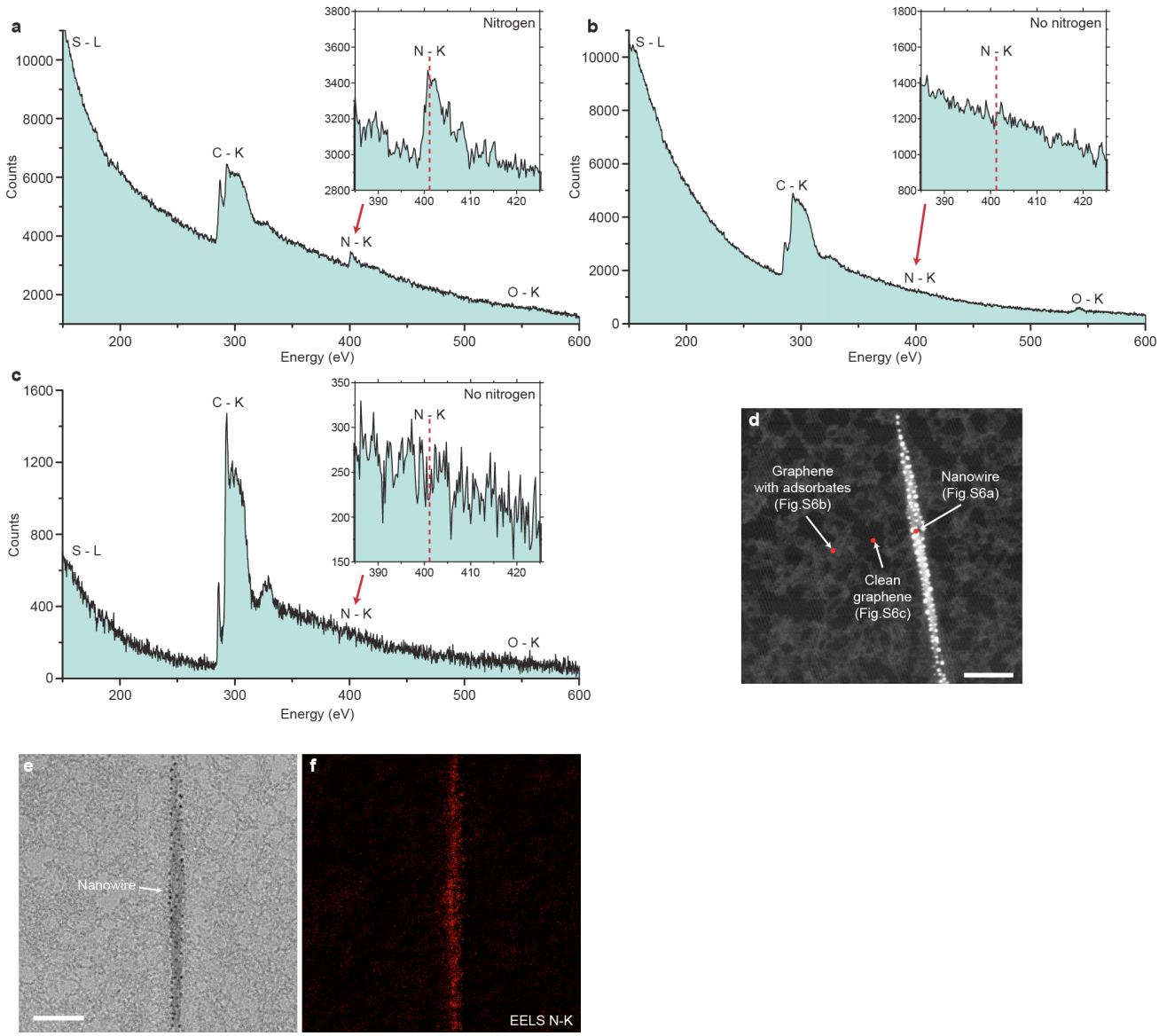

Supplementary Figure 6. Electron energy loss spectroscopic (EELS) analysis of the nanowires. **a–c,** EELS spectra of the nanowires on graphene (**a**), a graphene area with adsorbates (**b**), and a clean graphene area (**c**). The peaks indicate the presence of N within the nanowires. **d**, ADF TEM image showing three points for the EELS measurements in **a**, **b**, and **c**. Scale bar: 40 nm. **e–f**, EELS chemical mapping of the sample. The TEM image (**e**) and the energy-filtered TEM image at the N K-edge (**f**) are displayed. Scale bar: 25 nm.

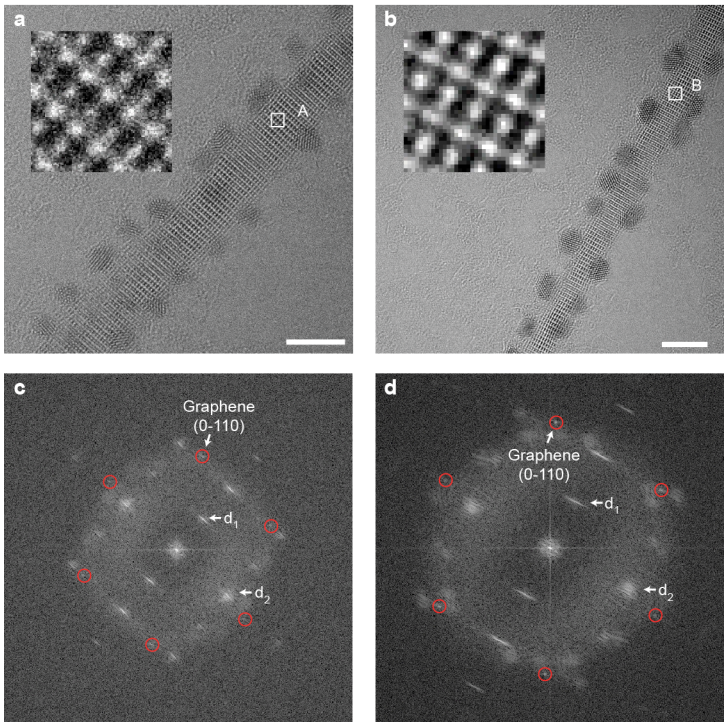

Supplementary Figure 7. Atomic-resolution TEM images of the nanowires. a–b, Atomic-resolution TEM images of the nanowires. The insets show enlarged views of the portions A and B, respectively. The inset in **a** is the same image as Fig. 2a. The scale bars indicate 5 nm. **c–d**, Fourier transforms of the TEM images. The first-order graphene diffraction spots are marked by red circles. The first-order diffraction spots from the nanowires are indicated by two arrows, d_1 and d_2. d_1 in **c**: 5.08 ± 0.01 Å, d_2 in **c**: 3.00 ± 0.12 Å, d_1 in **d**: 5.07 ± 0.01 Å, and d_2 in **d**: 3.00 ± 0.16 Å.

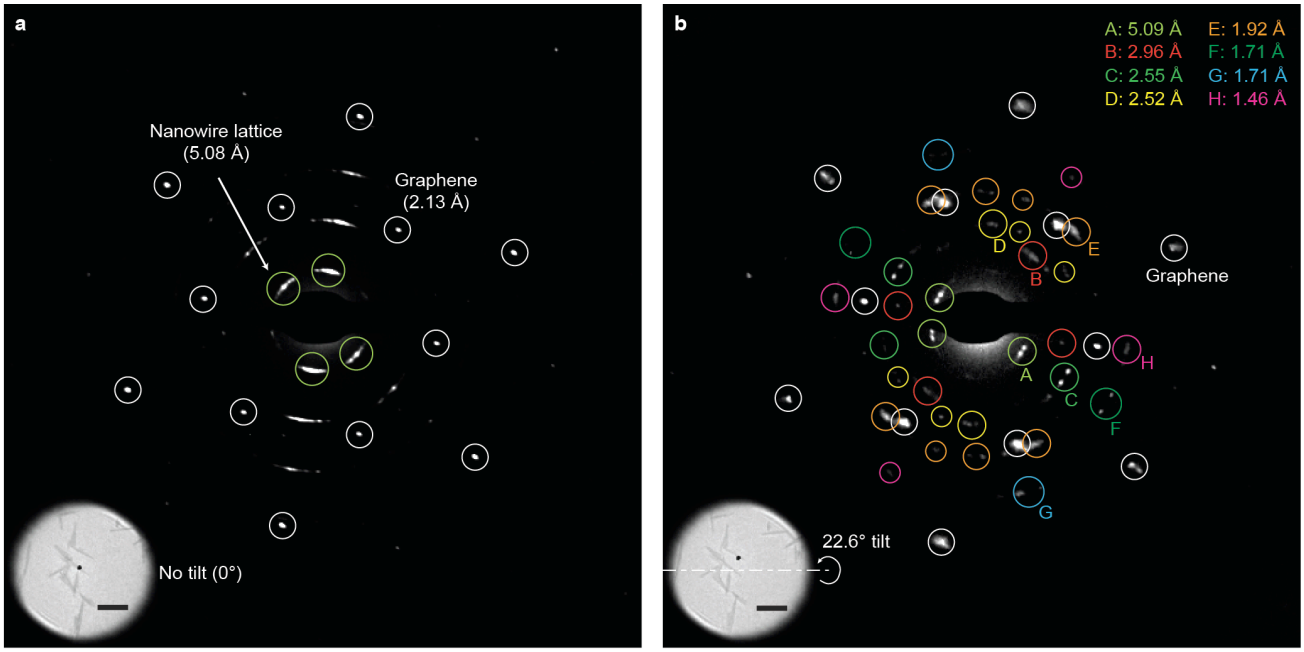

c

AuCN Miller indices	001	100	002	101	102	003	110	111	200	112
AuCN d-spacings (Å)	5.090	2.937	2.545	2.544	1.923	1.697	1.696	1.609	1.469	1.411
d-spacings from **b** (Å)	5.09 (A)	2.96 (B)	2.55 (C)	2.52 (D)	1.92 (E)	1.71 (F)	1.71 (G)	none	1.46 (H)	none
d-spacings from **Fig.2e** (Å)	5.08 (O)	2.95 (O)	2.54 (O)	2.53 (O)	1.92 (O)	none	none	none	1.47 (O)	none

Supplementary Figure 8. Comparison of d-spacings of an AuCN crystal and the nanowires. a–b, SAED patterns of a nanowire-graphene sample under no tilt (**a**) and a 22.6° tilt (**b**). The insets show the sample areas where the SAED patterns are measured. Scale bar: 100 nm. **c**, D-spacings obtained from an AuCN crystal and measured from SAED patterns of tilted nanowire samples. The matched d-spacings confirm that the synthesized nanowire is AuCN.

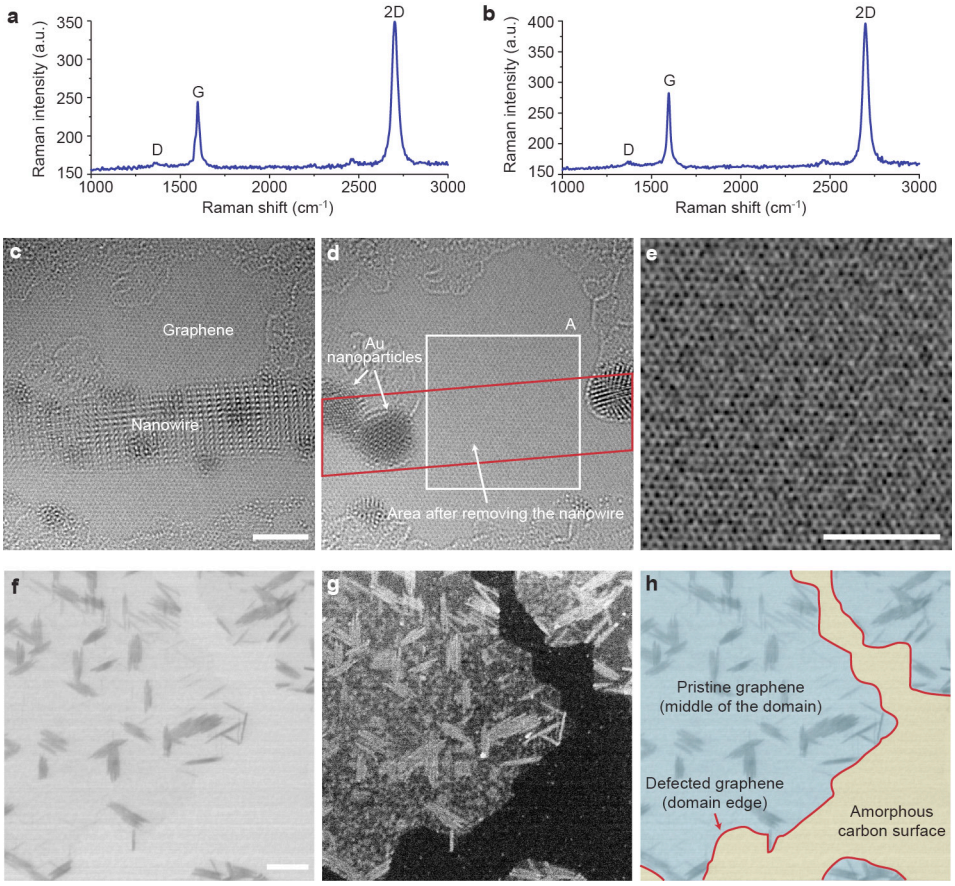

Supplementary Figure 9. Verification of the pristine state of graphene on which the nanowires are synthesized. a–b, Raman spectra of graphene before (**a**) and after (**b**) the nanowire growth. **c–e**, Atomic-resolution TEM images of a nanowire on graphene before (**c**) and after (**d**, **e**) removing the nanowire. The nanowire on graphene in the initial sample (**c**) is decomposed by e-beam irradiation (Fig. 4) in order to image the graphene surface underneath the nanowire (**d**). The enlarged and low-pass filtered image (**e**) of the section A in **d** confirms the pristine state of the graphene underneath the nanowire. The scale bars indicate 3 nm. **f–g**, Concurrently captured TEM (**f**) and SEM (**g**) images of the nanowires synthesized on graphene pieces transferred onto amorphous carbon films. The TEM (**f**) and SEM (**g**) images clearly show synthesized nanowires and graphene-covered areas, respectively. The scale bar indicates 100 nm. **h**, Coloured TEM image which differentiates graphene-covered areas from amorphous carbon films.

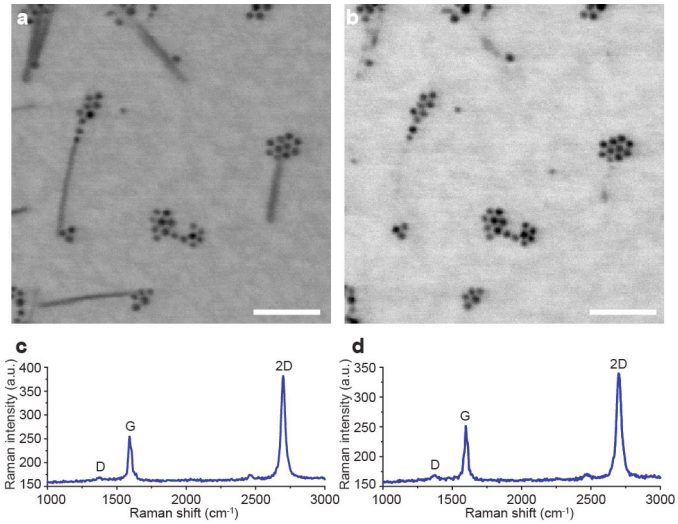

Supplementary Figure 10. Nanowire etching. a–b, TEM images of the sample before (**a**) and after (**b**) the nanowire etching process. The scale bar indicates 50 nm. **c–d**, Raman spectra of the sample before (**c**) and after (**d**) the nanowire etching process.

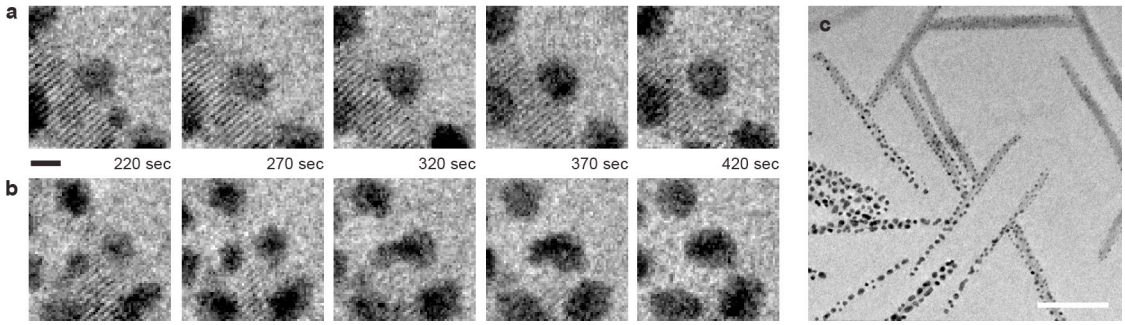

Supplementary Figure 11. Nanowire decomposition to Au nanoparticles under e-beam irradiation. a–b, A series of TEM images from Supplementary Video 1 for two different growth trajectories of Au nanoparticles: monomer addition (**a**) and coalescence (**b**). The scale bar indicates 2.5 nm. **c**, Au nanoparticle chains formed in the selected area (bottom-left corner) by irradiating the e-beam at the bottom-left corner. The scale bar indicates 50 nm.